

Cell-autonomous circadian clock of hepatocytes drives rhythms in transcription and polyamine synthesis

Ann Atwood^{a,1}, Robert DeConde^{b,1}, Susanna S. Wang^a, Todd C. Mockler^c, Jamal S. M. Sabir^d, Trey Ideker^b, and Steve A. Kay^{a,2}

^aSection of Cell and Developmental Biology, Division of Biological Sciences, and the Center for Chronobiology, University of California at San Diego, La Jolla, CA 92093-0130; ^bDepartments of Medicine and Bioengineering, University of California at San Diego, La Jolla, CA 92093-0063; ^cThe Donald Danforth Plant Science Center, St. Louis, MO 63132; and ^dDepartment of Biological Sciences, King Abdulaziz University, Jeddah, Kingdom of Saudi Arabia 21589

Contributed by Steve A. Kay, October 5, 2011 (sent for review August 3, 2011)

The circadian clock generates daily rhythms in mammalian liver processes, such as glucose and lipid homeostasis, xenobiotic metabolism, and regeneration. The mechanisms governing these rhythms are not well understood, particularly the distinct contributions of the cell-autonomous clock and central pacemaker to rhythmic liver physiology. Through microarray expression profiling in Met murine hepatocytes (MMH)-D3, we identified over 1,000 transcripts that exhibit circadian oscillations, demonstrating that the cell-autonomous clock can drive many rhythms, and that MMH-D3 is a valid circadian model system. The genes represented by these circadian transcripts displayed both cophasic and antiphasic organization within a protein-protein interaction network, suggesting the existence of competition for binding sites or partners by genes of disparate transcriptional phases. Multiple pathways displayed enrichment in MMH-D3 circadian transcripts, including the polyamine synthesis module of the glutathione metabolic pathway. The polyamine synthesis module, which is highly associated with cell proliferation and whose products are required for initiation of liver regeneration, includes enzymes whose transcripts exhibit circadian oscillations, such as ornithine decarboxylase and spermidine synthase. Metabolic profiling revealed that the enzymatic product of spermidine synthase, spermidine, cycles as well. Thus, the cell-autonomous hepatocyte clock can drive a significant amount of transcriptional rhythms and orchestrate physiologically relevant modules such as polyamine synthesis.

networks | chronobiology | resistance distance

Many aspects of mammalian physiology and behavior display circadian (~24-h) rhythms, including the sleep/wake cycle, blood pressure, heart rate, metabolism, and liver regeneration (1, 2). These rhythms are regulated by the circadian clock, which enables consolidation and coordination of physiological events to specific phases of the 24-h cycle in anticipation of daily environmental changes. Dysfunction of the clock is associated with serious human health conditions, including shift work syndrome, sleep disorders, increased risk of cancer, cardiovascular disease, and metabolic syndrome (1, 2).

The circadian clock is a self-sustaining, entrainable, cell-autonomous network of three interlocked transcriptional negative feedback loops (2). The primary loop consists of BMAL1/CLOCK transcriptional activators, which dimerize and turn on transcription of *Period* (*Per1*, *Per2*, and *Per3*) and *Cryptochrome* (*Cry1* and *Cry2*) genes through E-box elements. PER and CRY proteins dimerize and feed back to inhibit BMAL1/CLOCK activation. Two associate loops interlock with the core loop: the ROR/REV-ERB element (RRE) loop composed of ROR activators (ROR α , ROR β , and ROR γ) and REV-ERB repressors (REV-ERB α and REV-ERB β), which compete for RRE transcription factor binding sites (TFBS), and the D-box loop composed of the activator DBP and repressor E4BP4, which act through D-box TFBS (2).

In addition to internal regulation of clock genes, the clock also orchestrates circadian rhythms of output networks, which ultimately govern overt rhythms in physiology and behavior. Nearly all

mammalian cell types contain a circadian clock, producing at the organismal level a multioscillator system in which systemic and local circadian signals may jointly regulate physiology. This system can be divided into two main classes of clocks: the central pacemaker and peripheral clocks. The central pacemaker resides in the suprachiasmatic nucleus (SCN) and receives light input directly from the retina, entraining it directly to the light/dark cycle (1). The SCN acts to synchronize peripheral clocks in other tissues through systemic signals, and orchestrates rhythms in physiology. In contrast, the role of peripheral clocks remains to be elucidated. Despite ~10% of the genome displaying circadian rhythms in gene expression in many tissues, little overlap of rhythmic genes exists across tissues, suggesting that tissue-specific regulatory networks generate rhythms in local physiology (3, 4). In mice, disrupting the local liver clock abolishes circadian rhythms in many liver genes, even in the presence of a functional central pacemaker, implying a significant role for the liver clock in hepatic gene expression (5).

Rhythmic feeding behavior also represents a major entrainment signal for the hepatic clock. Restricting food access to the middle of the light period induces phase inversion of the liver clock in wild-type (WT) mice (6), and rhythmic feeding alone can drive oscillations in hepatic gene expression (7). When food is plentiful, feeding behavior is synchronized with the light/dark SCN-driven activity cycle. However, in conditions of scarcity or restricted access to food, feeding rhythms can be driven by the food-entrainable oscillator (FEO), which is independent of SCN light entrainment and is believed to involve multiple regions of the central nervous system (8–10). It remains unclear how hepatocytes balance the respective roles of systemic circadian regulation applied by the SCN and FEO vs. cell-autonomous regulation from the hepatic clock to generate circadian rhythms in liver functions.

To address the role of the cell-autonomous circadian clock, systemic influences need to be removed while still maintaining the integrity of the circadian clock and its physiological outputs. We selected the immortalized mouse cell line Met murine hepatocytes (MMH)-D3 as a candidate model system. Derived from the 3-d-old liver of transgenic c-Met mice (11), MMH-D3 is immortalized but not transformed, and maintains a high level of differentiation upon induction (11, 12), providing a system that reflects to a significant extent an *in vivo* hepatocyte.

We combined multiple analytic methods for the identification of circadian rhythms in large datasets. Using this pipeline, we reveal that MMH-D3 hepatocytes contain a functional cell-autonomous

Author contributions: A.A., R.D., S.S.W., and S.A.K. designed research; A.A., R.D., and S.S.W. performed research; A.A., R.D., and T.C.M. contributed new reagents/analytic tools; A.A., R.D., S.S.W., T.C.M., J.S.M.S., T.I., and S.A.K. analyzed data; and A.A., R.D., T.I., and S.A.K. wrote the paper.

The authors declare no conflict of interest.

Freely available online through the PNAS open access option.

¹A.A. and R.D. contributed equally to this work.

²To whom correspondence should be addressed. E-mail: skay@ucsd.edu.

This article contains supporting information online at www.pnas.org/lookup/suppl/doi:10.1073/pnas.1115753108/-DCSupplemental.

clock that can drive rhythms in gene expression of 1,130 transcripts, suggesting a significant role for this peripheral clock in the production of circadian physiology. We use these transcripts to demonstrate co- and antiphasic organization of circadian genes within the mouse protein interaction network, implying a general strategy of combining both positive and negative signals in the control of circadian processes. Last, we uncover cell-autonomous circadian cycles in polyamine biosynthesis, whose products are integral to initiating liver regeneration, suggesting a role for the hepatic clock in gating the initiation of liver regeneration (1, 2).

Results

Bioinformatics Pipeline for Identifying Circadian Rhythms. Recent reports demonstrate that circadian rhythm identification algorithms call different transcripts as cycling, even in the same dataset (4, 13). Further, existing methods show a dramatic reduction in the number of identified transcripts as the sampling rate decreases. Consequently, single methods applied to lower-resolution datasets produce very sparse lists of circadian calls (4), which may limit the types of further analyses run on these lists.

To address this issue, we constructed a bioinformatics pipeline for the identification of circadian rhythms in large datasets by combining two major analytic methods used in the analysis of circadian datasets: signal decomposition and model-matching (Fig. 1A) (4, 13, 14). The signal decomposition arm uses two Fourier analysis algorithms to identify cosine-based rhythms in an amplitude insensitive manner: Fisher's *G* test (4, 15) and Biological Rhythms Analysis Software System (BRASS) Fast Fourier transform nonlinear least squares (FFT NLLS) (16). The model-matching arm employs one algorithm, HAYSTACK, which uses user-defined models of a variety of phases and waveforms that extend beyond simple cosines—including spikes, box waves, rigid waves, and asymmetric rigid waves (Fig. S1) (14). Transcripts

identified by the model-matching and signal decomposition arms are combined to form the pipeline output.

To illustrate the effect of our pipeline on circadian transcript identification, we applied it to Hughes et al.'s (4) *in vivo* data from WT mouse liver (the Hughes WT liver dataset), which was collected at 1-h resolution over 48 h, and then to lower-resolution datasets created by subdividing the original at 2-, 3-, and 4-h intervals. Our pipeline identifies a greater number of transcripts than the 3,667 found by Hughes et al. (4) at 1-h resolution or either component analytic method individually (Fig. 1B and Fig. S2A–C). This increase in called transcripts mitigates the decline of circadian calls at lower sampling resolutions without sacrificing consistency, as evidenced by the >98% of 2-h circadian transcripts represented in the 1-h results (Fig. S2D–F).

Cell-Autonomous MMH-D3 Clock Drives Circadian Gene Expression.

To characterize the role of the cell-autonomous clock in MMH-D3 hepatocytes, we conducted a 2-h resolution microarray time-course experiment spanning 48 h and applied our pipeline for data analysis. We identified 1,130 transcripts displaying circadian expression: 801 transcripts called by model matching and 427 called by signal decomposition (Fig. 2A and Table S1). Algorithmic calls were validated using quantitative PCR (qPCR) for five clock genes, including at least one from each of the three interlocking feedback loops. The qPCR results corroborated the microarray traces for each of these genes (Fig. 2B–F) and the algorithm-predicted peak times of not only the first peak but also the second peak in the time course. Moreover, the phase differences between the clock genes representing each of the three negative feedback loops is consistent with the phase differences of the same genes in the Hughes WT liver dataset (Fig. S3A and B), and the MMH-D3 circadian transcripts display a bimodal distribution across the 24-h day, characteristic of circadian expression data (3, 5), confirming that the cell-autonomous clock is intact and can drive many rhythms in gene expression.

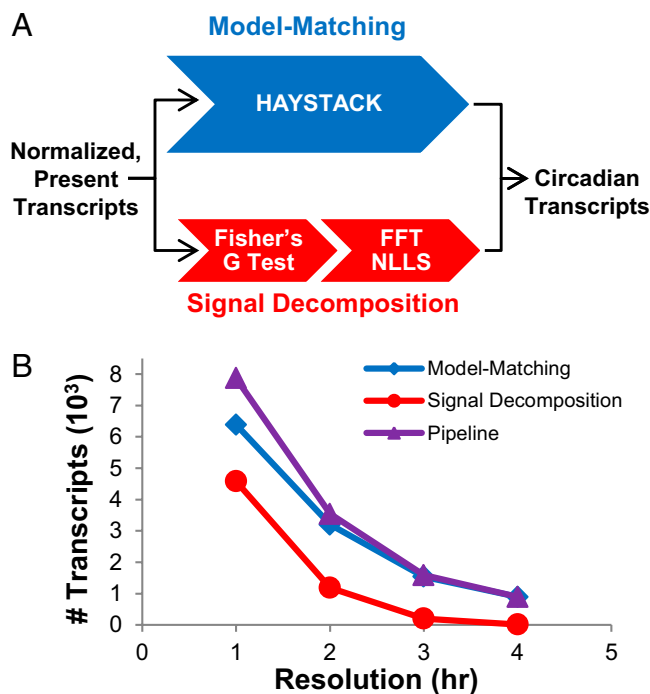


Fig. 1. Bioinformatics pipeline combines two analytic methods to increase circadian transcript yield. (A) Diagram depicting the pipeline component analytic methods: signal decomposition and model-matching algorithms. (B) Circadian transcripts identified by each analytic method (model-matching: blue, signal decomposition: red) and by the pipeline (purple) at decreasing resolution.

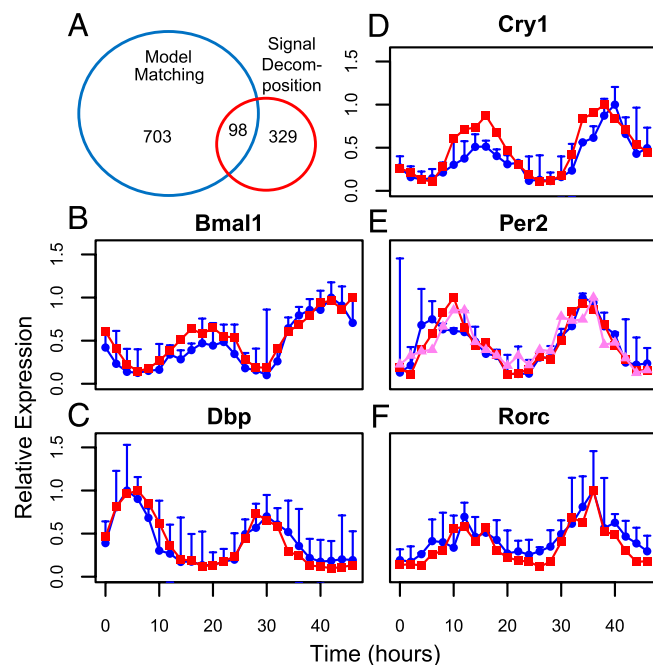


Fig. 2. MMH-D3 displays circadian rhythms of transcription. (A) MMH-D3 circadian transcript calls for each arm of pipeline. (B–F) qPCR (blue) and microarray transcript (red and pink) for indicated clock genes. Error bars on qPCR traces represent SD of replicates ($n = 3$).

network, circadian gene pairs display reduced shortest-path lengths between one another compared with noncircadian genes (Fig. 3A; Wilcoxon rank-sum test, $P < 10^{-15}$). We also examined closeness centrality—a measure inversely proportional to the mean shortest path between a given gene and all other genes in the network (21). On average, closeness was greater for circadian genes than noncircadian ones (Wilcoxon rank-sum test, $P = 0.017$; Fig. S4A). These results indicate that circadian genes are closer to one another and more centrally located in the network than noncircadian genes.

To determine if similarly phased genes were closer than those of disparate phase, we analyzed the resistance distance between pairs of circadian genes based on their difference in phase. Also referred to as commute time, the resistance distance is proportional to the average number of steps required for a random walk to run from one node to the other and back, and represents the strength of the overall connectivity between two nodes in a graph (22). We define the phase difference as the number of hours spanned by the smaller distance between the two phases on a 24-h clock, thus ranging from 0 to 12 h. Our analysis revealed that co- and antiphase gene pairs have significantly smaller mean resistance between them than those of intermediate phase differences (Fig. 3B). In addition, all phase differences showed significantly smaller mean resistance compared with permuted data (maximum $P < 0.05$ across the six bins), but to a greater extent for differences of 0–1 h and 9–12 h ($P < 0.01$ over 1,000 permutations; Methods). These results suggest a global organization of circadian genes by co- and antiphase relationships. The same property at the local level—analyzed using the distribution of phase differences among all first neighbors of each gene in the network—revealed a similar enrichment for co- and antiphase gene pairs (Fig. S4B).

To further examine the local circadian features of the network, we applied the MATISSE algorithm (23) to identify clusters of cophasic genes within the PPI network. The highest-scoring modules tended to be biphasic, consistent with the described proximity for co- and antiphase genes in the network, making large, separable clusters uncommon (Fig. 3C and D and Fig. S5). These modules reflect annotation clusters enriched in the MMH-D3 circadian transcript list identified by DAVID functional annotation clustering with GO and SwissProt keywords (Table S2), such as transcriptional regulators (transcriptional regulation: $P = 8.91 \times 10^{-6}$), chromatin-associated proteins (chromatin: $P = 2.08 \times 10^{-3}$), and regulators of phosphorylation (regulation of phosphorylation: $P = 6.72 \times 10^{-4}$; Fig. 3C) (24). These annotation clusters not only illustrate the breadth of the MMH-D3 circadian transcript list, but are consistent with our understanding of circadian regulation, because transcription, phosphorylation, and chromatin modification play key roles in regulating clock genes and clock function (2).

One module contained all of the clock genes in the core loop, and was dominated by transcriptional regulation (Fig. 3D) and illustrates the relationship of co- and antiphase genes in the network. This module suggests specific interactions for future circadian studies. Not only are components of transcription factor NF- κ B (NF- κ B1, NF- κ B2) represented, but also the regulator of its activating kinase (IKBKG) is also connected to clock genes through neighboring nodes. NF- κ B has been tenuously associated with the clock, but its regulatory interactions with the circadian system remain unclear (25, 26).

We compared our results for autonomous cycling calls in the MMH-D3 cell line with the 29 genes that Kornmann et al. (5) identified as having rhythms driven by systemic circadian regulation alone. The two lists displayed a moderately significant overlap of five genes (Per2, Fus, Hspa1b, Hspa8, and Heca; $P = 0.036$, Fisher's exact test), whereas the overlap of these 29 genes with the Hughes WT liver data were a more significant 21 genes ($P = 3.5 \times 10^{-8}$). These results support the conclusion that the Kornmann et al. (5) genes represent a largely distinct subset of the wild-type

circadian system (the systemic component) from those represented by the MMH-D3 cells (the cell-autonomous component). The five genes that do overlap—of which all but Heca appear in the PPI network and the MATISSE modules (Fig. 3D and Fig. S5)—display rhythms in both systemic and cell-autonomous conditions, and thus may represent interfaces between the two branches of circadian regulation.

Polyamine Synthesis Cycles in MMH-D3. DAVID pathway analysis (24) applied to the MMH-D3 circadian transcript list revealed enrichment in multiple pathways, including mammalian target of rapamycin (mTOR) signaling ($P = 3.2 \times 10^{-4}$), MAPK signaling ($P = 5.6 \times 10^{-3}$), and glutathione metabolism ($P = 5.6 \times 10^{-4}$)—specifically including the polyamine synthesis module (Fig. 4A, Table S3, and Fig. S6). The polyamines putrescine, spermidine, and spermine are small, aliphatic cations under physiological conditions that play key roles in cell proliferation and are essential for initiation of liver regeneration (27, 28). Our MMH-D3 hepatocyte time-course results displayed cell-autonomous circadian oscillations in the transcription of both the rate-limiting enzyme ornithine decarboxylase (Odc1) and the subsequent enzyme in the pathway, spermidine synthase (Srm; Fig. 4B and C) (27–29). Odc1 and Srm are also rhythmically expressed in the Hughes WT liver dataset (Fig. S7A and B) (4), but are not rhythmic in the livers of Vollmers et al.'s (7) *Cry1/Cry2* knockout or Miller et al.'s (30) *Clock* mutant mouse data (Fig. S7C–F), indicating that these rhythms are controlled by the circadian clock. Using mass spectrometry, we found that spermidine (the enzymatic product of

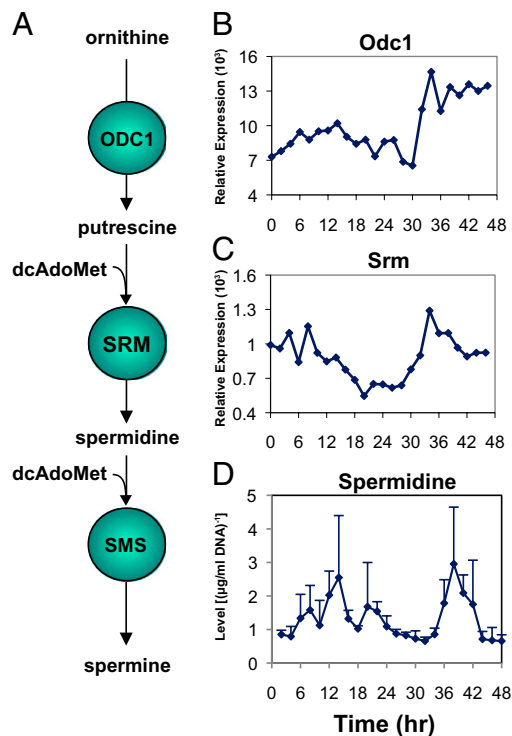


Fig. 4. Circadian rhythms of polyamine synthesis in both transcription and enzymatic activity. (A) Polyamine biosynthesis pathway. Ornithine is converted to putrescine (the first polyamine) by ornithine decarboxylase (ODC1). Putrescine is then converted to spermidine with the addition of decarboxylated S-adenosyl methionine (dcAdoMet) by spermidine synthase (SRM). Spermidine is then converted to spermine by spermine synthase (SMS). (B and C) Odc1 and Srm display circadian rhythms in MMH-D3 hepatocytes. (D) Spermidine displays circadian rhythmicity in MMH-D3 hepatocytes. Data points represent mean values for biological replicates ($n = 3$, except at hour 46, where $n = 2$) and error bars their SD.

SRM) exhibits circadian oscillations in MMH-D3 hepatocytes (Fig. 4D). Because the phases of *Odc1* and *Srm* transcriptional rhythms are coordinated, and ODC1 is the rate-limiting enzyme, oscillations in spermidine reflect not only the activity of SRM but ODC1 as well.

Discussion

In this study, using a bioinformatics pipeline that combines multiple analytic methods, we identified 1,130 circadian transcripts in MMH-D3 hepatocytes, indicating that the cell-autonomous hepatic clock can drive a significant proportion of circadian rhythms, and validating MMH-D3 as a model system for circadian biology.

The distribution of these genes within a mouse PPI network was both more central and concentrated than expected at random, and further organized to bring together co- and antiphasic genes. The proximity of antiphasic genes resembles relationships we observe within the circadian clock. Positive and negative components of individual clock loops are expressed at disparate phases and compete for the same binding sites, such as ROR activators and REV-ERB repressors competing for RRE binding sites (2). The phasic organization may reflect a general strategy of coupling positive and negative signals in the control and maintenance of specific circadian processes.

Last, we revealed robust cell-autonomous cycles in the polyamine synthesis module at both the transcriptional level and in enzymatic activity in MMH-D3 hepatocytes. Polyamines are strongly associated with cell proliferation, up-regulated in many cancers, and essential for liver regeneration, so circadian regulation of this pathway may gate the hepatocyte's permissibility to initiate liver regeneration (27–29).

Liver regeneration is known to be under circadian regulation, such that disruption of the clock retards liver regeneration and desynchronizes cell proliferation (31). Cell proliferation in regenerating hepatocytes is circadian and is gated by the kinase *Wee1* (31). Because polyamines are required for the initiation of liver regeneration, they may provide an upstream or additional mechanism for circadian regulation of the induction of the regeneration program. The mechanism by which polyamines initiate liver regeneration remains unclear, but they are essential to protein and DNA synthesis (32), and may play direct roles in stabilizing and transporting ribosomal RNA (32) as well as modulating protein–protein and protein–DNA interactions involved in transcription (28). Polyamines can also induce changes in DNA curvature to a more accessible conformation associated with transcription start sites (28). Thus, polyamines may act in the regulation of transcription in circadian output, including the induction of cell proliferation programs.

Cycling of *Odc1* and *Srm* transcripts may result from direct transcriptional regulation by the core clock loop, composed of BMAL1/CLOCK activators and PER/CRY repressors. Both *Odc1* and *Srm* are activated by c-Myc/MAX complexes binding to E-boxes in their regulatory regions (33, 34)—the same binding-site sequence used by BMAL1/CLOCK. It is known that BMAL1/CLOCK and c-Myc can regulate the same genes (35). Also, in MMH-D3 hepatocytes, *Odc1* and *Srm* transcripts peak at a similar time to the known BMAL1/CLOCK targets: *Dbp*, *Per2*, and *Rorc*. Furthermore, E-box regulation is enriched in circadian liver transcripts, but only when the local liver clock is intact, suggesting that much E-box-mediated transcriptional regulation requires a cell-autonomous liver clock (36). Further investigation should test the regulatory relationship between the core clock loop and polyamine synthesis.

Though polyamine synthesis can be induced in the in vivo liver by some systemic signals, including glucocorticoids, insulin, growth hormone, and food intake, previous studies did not address the intrinsic regulatory relationships within hepatocytes over circadian time (32). We present evidence of circadian regulation of polyamine synthesis in MMH-D3 hepatocytes by the cell-autonomous

clock, and, by extension, that the cell-autonomous clock may play a role in liver regeneration. In vivo, this cell-autonomous role likely integrates with systemic circadian regulatory signals to control polyamine synthesis and liver regeneration. Cell-autonomous circadian regulation may reflect the permissibility of hepatocytes to respond to systemic signals and liver injury at different times of the day, whereas systemic signals drive responses to changing external conditions.

Methods

MMH-D3 Culture. Cultures were maintained and differentiated before experiments in accordance with conditions in Amicone et al. (11). Cultures were synchronized via serum shock (37) and changed to serum-free medium for time-course collection. Cultures were incubated at 37 °C with 5% CO₂ for 12 h (microarrays) and 14 h (spermidine measurement) before the start of time-course collection.

MMH-D3 RNA and Microarray Preparation. Time-course collection began 12 h after synchronization of cultures. Every 2 h for 48-h duration, samples were collected in triplicate. Cell lysates were homogenized using Qiagen QIAshredder columns, and RNA was extracted using Qiagen RNeasy Miniprep Kit. Samples were normalized based on total RNA concentration, amplified, and applied to Affymetrix GeneChip Mouse 430 2.0 arrays per manufacturer specifications. This dataset is available at the Gene Expression Omnibus (GEO) database, www.ncbi.nlm.nih.gov/geo (accession no. GSE31049).

Microarray Analysis. The Hughes WT liver arrays were obtained from GEO accession no. GSE11923 (4) in vivo mouse liver dataset and processed using the methods described below. *Cry1*, *Cry2*^{-/-} mouse liver with ad libitum feeding dataset from Vollmers et al. (7) was obtained from GEO accession no. GSE13093 as a GCRMA-normalized expression matrix. *Clock* mutant liver dataset from Miller et al. (30) was obtained from GEO accession no. GSE3748 as a GCRMA-normalized expression matrix; plotted values represent the mean of two replicate arrays at each time point. All arrays were normalized using GCRMA and present/absent calls made by MAS5 performed in R/BioConductor. For further processing, only those transcripts that surpass the present threshold for datasets being analyzed were used.

Pipeline Analysis. Present, normalized transcripts for each dataset were applied to the statistical analysis pipeline depicted in Fig. 1A. For signal decomposition analysis, present, normalized datasets were subjected to Fisher's *G* test implemented in the GeneCycle package and a post hoc *q*-value estimate performed in GeneTS according to the methods of Hughes et al. (4) to call rhythmic transcripts at distinct Fourier frequencies corresponding to periods of 48, 24, 16, 12, 8, 6, 4.6, and 4 h. BRASS FFT NLLS was applied to transcripts with a Fisher's *G* test, *q* < 0.05, to define period and phase with a confidence interval of 0.95 (16). Circadian transcripts were those with a period of 20–30 h.

For model-matching analysis, HAYSTACK (<http://haystack.cgrb.oregonstate.edu>) was applied with user-defined models (Fig. S1), as described in Michael et al. (14). These models define cosine waveforms at 1-h increments from 20 to 28 h and alternate waveforms with 24-h periods (Fig. S1). Correlation cutoffs corresponding to a pseudo-FDR < 0.05 were determined for the MMH-D3 dataset and the Hughes WT liver dataset using 500 and 1,000 permutations, respectively, for each resolution analyzed. The correlation cutoffs were: MMH-D3 0.6067, Hughes WT liver 1-h resolution 0.4549, Hughes WT liver 2-h resolution 0.6314, Hughes WT liver 3-h resolution 0.7639, and Hughes WT liver 4-h resolution 0.8520. When a transcript was called by both analytical arms of the pipeline, the signal decomposition phase value was used.

Functional Annotation. DAVID functional annotation clustering was performed using GO and SwissProt keywords with medium clustering stringency. Clusters with enrichment scores > 1.3 (corresponding to mean *P* < 0.05) were significant (24). DAVID pathway analysis was performed using KEGG PATHWAY. Overrepresented pathways displayed a *P* < 0.05 and fold enrichment ≥ 1.5 (24). GO annotation for assessment of glycolysis and oxidative respiration performed in R/Bioconductor using the GStats package (38).

qPCR. Quantitative real-time PCR was performed on the same RNA samples as used for MMH-D3 microarrays according to the methods of Liu et al. (37) using TaqMan assays and normalized based on GAPDH levels. Three replicates of each qPCR reaction were performed. Relative expression values are reported in percentage of maximum mean normalized values. Data points

reflect the percent expression mean of replicates ($n = 3$), and error bars represent SD of replicates.

Spermidine Measurement. Samples were collected starting 14 h after synchronization of differentiated MMH-D3 cultures. At 2-h intervals for a duration of 48 h, three live-cell pellets, each representing 10^6 cells, were collected, except for time point 23 (hour 46) in which two live-cell pellets were collected. To collect cell pellets, cultures were washed three times with cold (4 °C) PBS, trypsinized using 0.25% trypsin with EDTA, washed with PBS, flash-frozen in liquid nitrogen, and stored at -80 °C. Biochemical extraction, mass spectrometry, and metabolite quantification were performed by Metabolon (Metabolon, Inc.) as described previously (39, 40). Sample measurements were normalized by DNA concentration from each cell pellet sample. Spermidine levels represent the mean of DNA-normalized samples at each time point, and error bars are their SD.

Protein–Protein Interaction Network Construction and Analysis. Network visualization of protein–protein interactions and MMH-D3 circadian phases was performed using Cytoscape 2.8.1 (<http://www.cytoscape.org/>) (41). To construct the mouse PPI network, we pulled all mouse-specific interactions from iRefIndex (version 8.0), a metadata database that combines interaction data from 10 primary databases (20) (*SI Methods*). To generate consistent network statistics regarding direct PPIs, redundant edges were collapsed into a single (undirected) edge, excluding edges representing “colocalization,” and we replaced nodes for protein complexes with all pairwise edges, resulting in an undirected network of 7,052 genes and 91,457 edges. Of the 930 MMH-D3 circadian genes (1,130 transcripts), 297 mapped to nodes in the network by Entrez Gene IDs. This larger network was used for the enrichment analysis of first neighbors, which does not require a single connected component. The shortest path, closeness centrality, resistance distance, and MATISSE analyses were applied to the largest connected component—meaning all pairs of genes in the subnetwork were connected by at least one path—of this network, consisting of 5,302 genes, 230 of which were circadian.

Resistance distance was calculated using the Moore–Penrose inverse of the normalized Laplacian matrix of the largest connected component of the PPI network. The normalized Laplacian of a graph is defined as $L = I - D^{-1}A$, where I is the identity matrix, D is the degree matrix of the graph (a diagonal matrix where d_{ii} is the degree of node i), and A is the graph adjacency matrix. Mean values were calculated for all pairs of genes within each phase-difference bin, and permutation analysis was done using 1,000 permutations of the phase values across the network. P values for each bin were calculated as the proportion of the permuted bin means exceeding the mean value for that bin from the nonrandomized results.

For the analysis of first neighbors (Fig. S4B), the sets of first neighbors of every gene in the network were found, and the phase differences between all pairs of circadian genes within each neighborhood set were counted and summed across all neighborhoods. These sums were then normalized by the total number of circadian pairs in all of the neighborhoods, providing a distribution across the phase differences. This same analysis was performed on 1,000 permuted networks with the measured phase values randomly assigned to different nodes, and signed P values were calculated using the proportion of times the value in a given bin in the measured distribution was greater or less than the same value in the permuted distributions.

The MATISSE algorithm (<http://acgt.cs.tau.ac.il/matisse/>) (23) was applied to identify cophasic modules. We used the custom MATISSE algorithm from the program, which allowed us to specify a similarity matrix for the circadian nodes in the network, which we defined as the phase difference, normalized to the range 0–1, and raised to the fourth power. The exponent served to increase the relative similarity score of cophasic genes from those with phases differing by ≥ 3 h. Other chosen parameters were the minimum seed size (five nodes), the maximum seed size (five nodes), the seed strategy (all neighbors), the minimum module size (five nodes), and the maximum module size (30 nodes).

ACKNOWLEDGMENTS. This work was supported in part by National Institutes of Health Grants R01 GM074868, R01 MH051573, and P50GM085764 (to S.A.K.) and Cell and Molecular Genetics Training Program National Institutes of Health Grant GM07240 (to A.A.).

- Hastings MH, Reddy AB, Maywood ES (2003) A clockwork web: Circadian timing in brain and periphery, in health and disease. *Nat Rev Neurosci* 4:649–661.
- Zhang EE, Kay SA (2010) Clocks not winding down: Unravelling circadian networks. *Nat Rev Mol Cell Biol* 11:764–776.
- Panda S, et al. (2002) Coordinated transcription of key pathways in the mouse by the circadian clock. *Cell* 109:307–320.
- Hughes ME, et al. (2009) Harmonics of circadian gene transcription in mammals. *PLoS Genet* 5:e1000442.
- Korrmann B, Schaad O, Bujard H, Takahashi JS, Schibler U (2007) System-driven and oscillator-dependent circadian transcription in mice with a conditionally active liver clock. *PLoS Biol* 5:e34.
- Damiola F, et al. (2000) Restricted feeding uncouples circadian oscillators in peripheral tissues from the central pacemaker in the suprachiasmatic nucleus. *Genes Dev* 14:2950–2961.
- Vollmers C, et al. (2009) Time of feeding and the intrinsic circadian clock drive rhythms in hepatic gene expression. *Proc Natl Acad Sci USA* 106:21453–21458.
- Fuller PM, Lu J, Saper CB (2008) Differential rescue of light- and food-entrainable circadian rhythms. *Science* 320:1074–1077.
- Storch KF, Weitz CJ (2009) Daily rhythms of food-anticipatory behavioral activity do not require the known circadian clock. *Proc Natl Acad Sci USA* 106:6808–6813.
- Carneiro BT, Araujo JF (2009) The food-entrainable oscillator: A network of interconnected brain structures entrained by humoral signals? *Chronobiol Int* 26:1273–1289.
- Amicone L, et al. (1997) Transgenic expression in the liver of truncated Met blocks apoptosis and permits immortalization of hepatocytes. *EMBO J* 16:495–503.
- Mancone C, et al. (2010) Proteomic analysis reveals a major role for contact inhibition in the terminal differentiation of hepatocytes. *J Hepatol* 52:234–243.
- Khan S, Rowe SC, Harmon FG (2010) Coordination of the maize transcriptome by a conserved circadian clock. *BMC Plant Biol* 10:126.
- Michael TP, et al. (2008) Network discovery pipeline elucidates conserved time-of-day-specific cis-regulatory modules. *PLoS Genet* 4:e14.
- Wichert S, Fokianos K, Strimmer K (2004) Identifying periodically expressed transcripts in microarray time series data. *Bioinformatics* 20:5–20.
- Brown PE (2004) Biological Rhythms Analysis Software System. Available at: <http://millar.bio.ed.ac.uk/Downloads.html>.
- Bissell DM, Levine GA, Bissell MJ (1978) Glucose metabolism by adult hepatocytes in primary culture and by cell lines from rat liver. *Am J Physiol* 234:C122–C130.
- Covington MF, Maloof JN, Straume M, Kay SA, Harmer SL (2008) Global transcriptome analysis reveals circadian regulation of key pathways in plant growth and development. *Genome Biol* 9:R130.
- Keegan KP, Pradhan S, Wang JP, Allada R (2007) Meta-analysis of *Drosophila* circadian microarray studies identifies a novel set of rhythmically expressed genes. *PLoS Comput Biol* 3:e208.
- Razick S, Magklaras G, Donaldson IM (2008) iRefIndex: A consolidated protein interaction database with provenance. *BMC Bioinformatics* 9:405.
- Newman MEJ (2005) A measure of betweenness centrality based on random walks. *Soc Networks* 27:39–54.
- Klein DJ, Randić M (1993) Resistance distance. *J Math Chem* 12:81–95.
- Ulitsky I, Shamir R (2007) Identification of functional modules using network topology and high-throughput data. *BMC Syst Biol* 1:8.
- Huang W, Sherman BT, Lempicki RA (2009) Systematic and integrative analysis of large gene lists using DAVID bioinformatics resources. *Nat Protoc* 4:44–57.
- Kuo TH, Pike DH, Bezaeipour Z, Williams JA (2010) Sleep triggered by an immune response in *Drosophila* is regulated by the circadian clock and requires the NfκB Relish. *BMC Neurosci* 11:17.
- Cecon E, Fernandes PA, Pinato L, Ferreira ZS, Markus RP (2010) Daily variation of constitutively activated nuclear factor kappa B (NFκB) in rat pineal gland. *Chronobiol Int* 27:52–67.
- Alhonen L, et al. (2002) Polyamines are required for the initiation of rat liver regeneration. *Biochem J* 362:149–153.
- Thomas T, Thomas TJ (2003) Polyamine metabolism and cancer. *J Cell Mol Med* 7:113–126.
- Jänne J, et al. (2005) Animal disease models generated by genetic engineering of polyamine metabolism. *J Cell Mol Med* 9:865–882.
- Miller BH, et al. (2007) Circadian and CLOCK-controlled regulation of the mouse transcriptome and cell proliferation. *Proc Natl Acad Sci USA* 104:3342–3347.
- Matsuo T, et al. (2003) Control mechanism of the circadian clock for timing of cell division in vivo. *Science* 302:255–259.
- Russell DH, Byus CV, Manen CA (1976) Proposed model of major sequential biochemical events of a trophic response. *Life Sci* 19:1297–1305.
- Forsell TP, Rimpì S, Nilsson JA (2010) Chemoprevention of B-cell lymphomas by inhibition of the Myc target spermidine synthase. *Cancer Prev Res (Phila)* 3:140–147.
- Bello-Fernandez C, Packham G, Cleveland JL (1993) The ornithine decarboxylase gene is a transcriptional target of c-Myc. *Proc Natl Acad Sci USA* 90:7804–7808.
- Sherman H, Froy O (2008) Expression of human beta-defensin 1 is regulated via c-Myc and the biological clock. *Mol Immunol* 45:3163–3167.
- Bozek K, Rosahl AL, Gaub S, Lorenzen S, Herzog H (2010) Circadian transcription in liver. *Biosystems* 102:61–69.
- Liu AC, et al. (2008) Redundant function of REV-ERBα and β and non-essential role for Bmal1 cycling in transcriptional regulation of intracellular circadian rhythms. *PLoS Genet* 4:e1000023.
- Falcon S, Gentleman R (2007) Using GOSTats to test gene lists for GO term association. *Bioinformatics* 23:257–258.
- Evans AM, DeHaven CD, Barrett T, Mitchell M, Milgram E (2009) Integrated, non-targeted ultrahigh performance liquid chromatography/electrospray ionization tandem mass spectrometry platform for the identification and relative quantification of the small-molecule complement of biological systems. *Anal Chem* 81:6656–6667.
- Ryals J, Lawton K, Stevens D, Milburn M (2007) Metabolon, Inc. *Pharmacogenomics* 8:863–866.
- Smoot ME, Ono K, Ruscheinski J, Wang PL, Ideker T (2011) Cytoscape 2.8: New features for data integration and network visualization. *Bioinformatics* 27:431–432.